Exploring the high load potential of diesel-methanol dual-fuel operation with Miller cycle, EGR, and intake air cooling on a heavy-duty diesel engine

Wei Guan[1,2], Xinyan Wang[1], Hua Zhao[1] , Haifeng Liu[3]

[1]Brunel University London, London, United Kingdom

[2]Guangxi Yuchai Machinery Company, Yulin, China

[3]Tianjin University, Tianjin, China

Abstract

Legislations concerning emissions from heavy-duty (HD) diesel engines are becoming increasingly stringent. This requires conventional diesel combustion (CDC) to be compliant using costly and sophisticated aftertreatment systems. Preferably, Diesel-methanol dual-fuel (DMDF) is one of the suitable alternative combustion modes as it can potentially reduce the formation of NO_x and soot emissions which characterised the diesel mixing-controlled combustion. This is primarily due to the high latent heat of vaporisation and oxygen content of the methanol fuel. At high engine loads, however, the potential of DMDF operation is constrained by the excessive combustion pressure rise rate (PRR) and peak in-cylinder pressure, which limits both the engine efficiency and the percentage of methanol that can be used. For the first time, experimental studies were conducted to explore advanced combustion control strategies such as Miller cycle, exhaust gas recirculation (EGR), and intake air cooling for improving upon high-load DMDF combustion. Experiments were carried out at 1200 rpm and 18 bar indicated mean effective pressure (IMEP) on a single cylinder HD diesel engine, which equipped with a high pressure common rail diesel injection, a methanol port fuel injection, and a variable valve actuation system on the intake camshaft.

Results showed that the methanol energy fraction (MF) of a conventional DMDF operation with a baseline intake valve closing (IVC) timing was limited to 28%. This was due to the high combustion temperature at a high load which advanced the ignition timing of the premixed charge, resulting in high levels of PRR. The application of lower effective compression ratio (ECR) and intake air temperature (T_{int}) effectively decreased the compression temperature, which successfully delayed the ignition timing of the premixed charge. This allowed for a more advanced diesel injection timing to achieve improvement in the thermal efficiency and potentially enabled a higher methanol substitution ratio. Although the introduction of EGR demonstrated very slight impact on the ignition timing of the premixed charge, a higher net indicated efficiency was observed due to a relatively lower local combustion temperature which reduced heat transfer loss. Moreover, the optimised DMDF operation allowed a higher MF of 40% to be used at an ECR of 14.3 and T_{int} of 305 K and achieved the highest net indicated efficiency of 47.4%, improving by 3.7% and 2.6% respectively when compared to the optimised CDC (45.7%) and conventional DMDF (46.2%). This improvement was accompanied with a reduction of 37% in NOx emissions and little impact on soot emissions in comparison with the CDC.

Keywords

Heavy-duty diesel engine, methanol, dual-fuel, Miller cycle, EGR, intake air cooling

1. Introduction

According to the most comprehensive assessment of climate change undertaken by the Intergovernmental Panel on Climate Change, the global warming is strongly related to the burning of fossil fuels which add a substantial amount of greenhouse gases (GHG) such as CO_2 into the atmosphere [1]. Among different sources, CO_2 emissions produced by transportation are the largest sector [2]. In particular, the commercial sector, namely HD trucks, with 4% of the total number of on-road vehicles, accounts for 18% of the fuel consumption and CO_2 emissions within the transportation sector [3]. In addition to GHG emissions, pollutants such as NO_x and soot are of increasing concern as they have significantly harmful impact on human health and environment. These issues are driving the development of powertrain technology and the exploration of alternative advanced combustion modes.

Conventional diesel combustion (CDC) is suffered from the typical NO_x-soot trade-off. Their formation is due to the fact that the non-premixed diffusion-controlled combustion is characterised by a wide range of local in-cylinder gas temperatures and equivalence ratios [4]. To comply with strict emissions regulations, costly and sophisticated aftertreatment systems are essential [5].

In last few decades, numerous research has focused on low temperature combustion (LTC) modes, which includes Homogeneous Charge Compression Ignition (HCCI) [6], Premixed Charge Compression Ignition (PCCI) [7], Partially Premixed Charge Compression Ignition (PPCI) [8], Modulated Kinetics (MK) [9], and Uniform Bulky Combustion System (UNIBUS) [10]. These allow a higher degree of combustion phasing control at low and medium loads and have shown their potential to achieve simultaneous low levels of NO_x and soot emissions. However, these combustion modes suffer from high unburned HC and CO emissions, lack of combustion phasing control, and limited load range operation.

Interest in renewable alternatives for heavy-duty applications to partially replace fossil fuel has achieved fast grow in recent years. Dual-fuel (DF) combustion, such as Reactivity Controlled Compression Ignition (RCCI), has been researched as a method to effectively use alternative fuels in conventional diesel engines and developed to overcome the previously mentioned issues [11–13]. The method separates the fuel delivery, port fuel injection of the low reactivity fuel such as gasoline, natural gas, methanol, and ethanol while directly injecting the high reactivity fuel (e.g. diesel) to serve as the ignition source. Among the low reactivity fuels, methanol is one of the most promising alternative fuels for internal combustion engines as it can be produced from renewable sources. Methanol can be produced from various resources including biomass, natural gas, hydrogen, coal, and coke-oven gas, which thus can be a superior fuel for long-term and widespread replacement of conventional fossil fuels. Methanol is also a high oxygen content fuel with high latent heat of vaporisation, having the potential to reduce NOx and smoke emissions [14–16].

This concept has been shown to enable reactivity stratification controlled by the direct-injection of diesel, allowing for a wide range of operation with acceptable pressure rise rate [17,18]. A number of studies revealed that an optimised DF combustion can achieve lower levels of NO_x and soot, and a better thermal efficiency in comparison with the CDC operation [19–21]. However, high-load DF operations suffer from high levels of PRR and peak in-cylinder pressure limitations due to the autoignition and fast combustion of the premixed fuel, which associated with the high combustion temperature at a high load [14,22].

The use of EGR has been proven as an effective method to extend the high-load DF operation. This is associated with a reduction in the combustion temperature due to the increased specific heat capacity and dilution level of the in-cylinder charge [23,24], which delays the ignition time of the premixed fuel and thus allows for a high-load DF operation with low levels of PRR and NO_x emissions [25–28]. Additionally, the application of a lower compression ratio has attracted more attention for the suppression of in-cylinder gas pressure and temperature at high load operation [29–31]. Particularly, the use of Miller cycle to achieve variable compression ratio via early intake valve closing (EIVC) or late intake valve closing timings (LIVC) has been mostly focused on [32–34]. This is attributed to the effectiveness of Miller cycle in reducing the in-cylinder gas temperature and pressure during compression strokes, allowing for a more flexible combustion control of both injected fuels over the engine cycles. On the other hand, the delayed intake valve closure decreases the in-cylinder charge density and oxygen availability. This can increase the average in-cylinder gas temperature due to lower total heat capacity [35] and adversely affect combustion process due to lower air-fuel ratio [36], potentially decreasing the engine efficiency [37].

Moreover, the intake air cooling is another effective combustion control strategy used for overcoming the limitation of high load DF combustion. Pedrozo et al. [30] experimentally investigated ethanol-diesel dual-fuel operating with Miller cycle and intake air cooling at high load. They found that a reduction in the intake air temperature can suppress the early ignition of ethanol, allowing for a substantial improvement in the maximum ethanol energy fraction, net indicated efficiency, and NO_x emissions. Wang et al. [38] and Varde [16] also revealed that decreasing intake air temperature can effectively minimise the maximum in-cylinder gas pressure (P_{max}) and PRR by delaying the ignition timing of the premixed fuel derived from the port-injection.

Considering the majority of previous works were performed individually to investigate the effects of EGR, intake cooling, and Miller cycle on the DMDF operation, a systematic experimental study was carried out on a single cylinder heavy-duty diesel engine to comprehensively analysed their potential for increasing the maximum net indicated efficiency. Advanced combustion control strategies were explored to improve the high load DMDF operation with high efficiency and low levels of NO_x and soot emissions. To the best of our knowledge, the current work is the first attempt to experimentally investigate and compare the potential of high load methanol-diesel dual-fuel operation with EGR, Miller cycle, and intake air cooling.

The experiments were performed at 1200 rpm and 18 bar IMEP with varying diesel injection timings to up to the PRR and in-cylinder pressure limitations. Specifically, the low reactivity fuel via port fuel injection was methanol while the diesel fuel was directly injected into the cylinder as an ignition source. The effects of methanol energy fraction, EGR, Miller cycle, and intake air cooling were evaluated. The potential of DMDF operation with Miller cycle and intake air cooling was analysed. Finally, the optimised advanced DMDF results were compared against the optimised CDC and conventional DMDF operations.

2. Experimental setup

2.1 Engine specifications and experimental facilities

Figure 1 shows the schematic diagram of the single cylinder heavy-duty diesel engine. A Froude Hofmann AG150 eddy current dynamometer was coupled to absorb the engine power output. Table 1 outlines the base hardware specifications of the test engine. The combustion system was designed based on a production Yuchai YC6K 6-cylinder diesel engine, which consisted of a 4-valve swirl-oriented cylinder head and a stepped-lip piston bowl design with a geometric compression ratio of 16.8. The bottom end/short block was AVL-designed with two counter-rotating balance shafts.

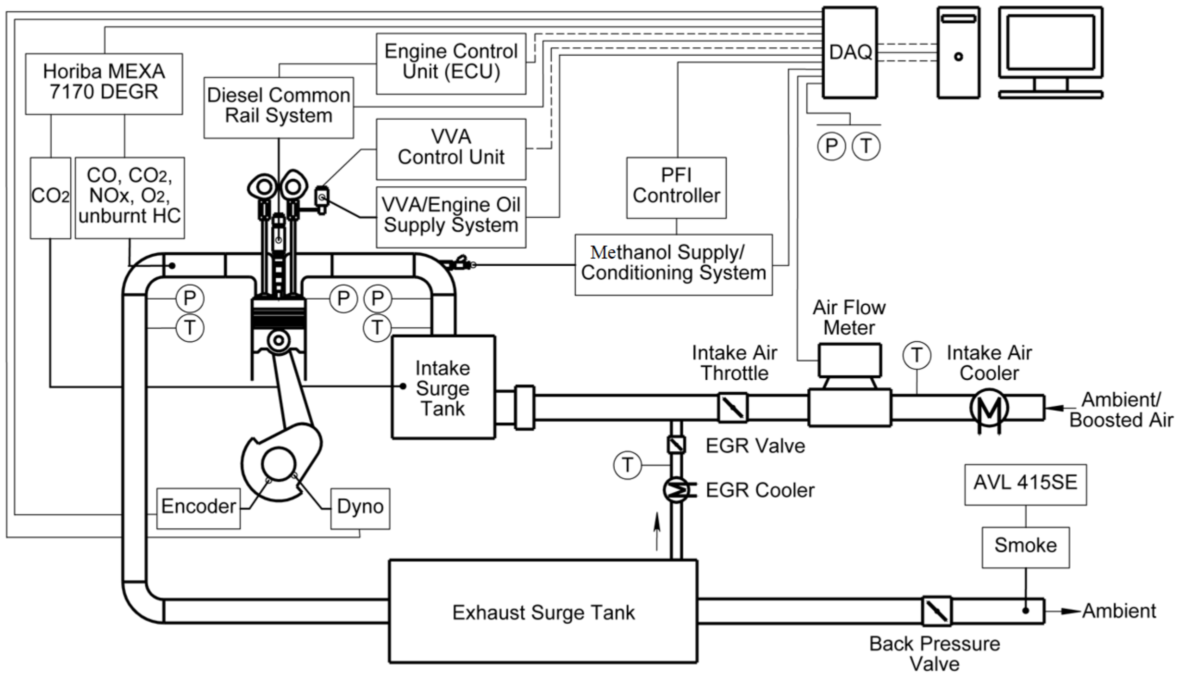

Figure 1. Layout of the engine experimental setup.

Table 1. Specifications of the test engine.

Displaced Volume	2026 cm^3
Stroke	155 mm
Bore	129 mm
Connecting Rod Length	256 mm
Geometric Compression Ratio	16.8
Number of Valves	4
Piston Type	Stepped-lip bowl
Diesel Injection System	Bosch common rail
Nozzle design	8 holes, 0.176 mm hole diameter, included spray angle of 150°
Maximum fuel injection pressure	2200 bar
Maximum in-cylinder pressure	180 bar

The compressed air was supplied by an AVL 515 sliding vanes supercharger with closed loop control. Two surge tanks were installed to damp out the strong pressure fluctuations in intake and exhaust manifolds. The intake manifold pressure was finely controlled by a throttle valve located upstream of the intake surge tank. An Endress+Hauser Proline t-mass 65F thermal mass flow meter was used to measure the fresh air mass flow rate. An electronically controlled butterfly valve located downstream of the exhaust surge tank was used to independently control the exhaust back pressure. High-pressure loop cooled external EGR was introduced to the engine intake manifold located between the intake surge tank and throttle by using a pulse width modulation-controlled EGR valve and the pressure differential between the intake and exhaust manifolds. Coolant and oil pumps were driven by separate electric motors. Water cooled heat exchangers were used to control the temperatures of the boosted intake air and external EGR as well as engine coolant and lubricating oil. The coolant and oil temperatures were kept within 356 ± 2 K. The oil pressure was maintained within 4.0 ± 0.1bar throughout the experiments. The specifications of the measurement equipment can be found in Appendix A.

2.2 Fuel properties and fuelling system

Table 2 shows the diesel and methanol fuel properties. During the dual-fuel operation, methanol was injected through a port fuel injector. The desired methanol energy fraction was achieved via adjusting the PFI pulse width controlled by an injector driver. The methanol mass flow rate ($\dot{m}_{methanol}$) was obtained from an injector calibration curve determined with a semi-microbalance with an accuracy of ±0.1 mg. Methanol injection pressure was continuously monitored to maintain a constant relative pressure of 3.0 bar across the injector. The methanol temperature was kept between 292 and 298 K through a heat exchanger.

Table 2. Fuel properties of diesel and methanol.

Properties	Red diesel	Methanol
Density at 293 K (ρ)	0.827 kg/dm3	0.791 – 0.794 g/mL 20 °C

Cetane number	> 45	4
Research octane number (RON)	n/a	109
Water content	< 0.20 g/kg	NMT 0.1% wt (1000 ppm)
Heat of vaporisation	270 kJ/kg	1.11 MJ/kg
Carbon mass content	86.6%	37.5 (wt.%)
Hydrogen mass	13.2%	12.5%
Oxygen mass content	0.2%	50%
Molecular formula	$CH_{1.825}O_{0.0014}$	CH_3OH
Lower heating value (LHV)	42.9 ×10^6 J/kg	20.27×10^6 J/kg

The diesel fuel injection parameters such as injection pressure, start of injection (SOI), and the number of injections were controlled by a dedicated electronic control unit (ECU). During the experiments, the diesel fuel rate ($\dot{m}_{diesel}$) was injected into the engine by a high-pressure solenoid injector through a high pressure pump and a common rail with a maximum fuel pressure of 2200 bar. The fuel consumption was determined by measuring the total fuel supplied to and from the high pressure pump and diesel injector via two Coriolis flow meters.

The methanol energy fraction (MF) was defined as the ratio of the energy content of the methanol to the total fuel energy by

$$MF\% = \frac{\dot{m}_{methanol}LHV_{methanol}}{\dot{m}_{methanol}LHV_{methanol} + \dot{m}_{diesel}LHV_{diesel}} \tag{1}$$

The actual lower heating value of the in-cylinder fuel mixture (LHV_{DF}) was calculated as

$$LHV_{DF} = \frac{(\dot{m}_{methanol}LHV_{methanol}) + (\dot{m}_{diesel}LHV_{diesel})}{\dot{m}_{methanol} + \dot{m}_{diesel}} \quad (2)$$

2.3 Variable valve actuation system

The engine was equipped with a prototype hydraulic lost-motion VVA system, which incorporated a hydraulic collapsing tappet on the intake valve side of the rocker arm. The VVA system allowed for the adjustment of the IVC timing and thus enabled Miller cycle operation. The intake valve opening (IVO) and closing (IVC) of the baseline case were set at 367 and -178 crank angle degrees (CAD) after top dead centre (ATDC), respectively. All valve events were considered at 1 mm valve lift and the maximum intake valve lift event was set to 14 mm. Figure 2 shows the intake and exhaust valve profiles for the baseline and Miller cycle operations. The effective compression ratio, ECR, was calculated as

$$ECR = \frac{V_{ivc\_eff}}{V_{tdc}} \quad (3)$$

where V_{tdc} is the cylinder volume at top dead centre (TDC) position, and V_{ivc_eff} is the effective cylinder volume where the in-cylinder compressed air pressure is extrapolated to be identical to the intake manifold pressure [39,40].

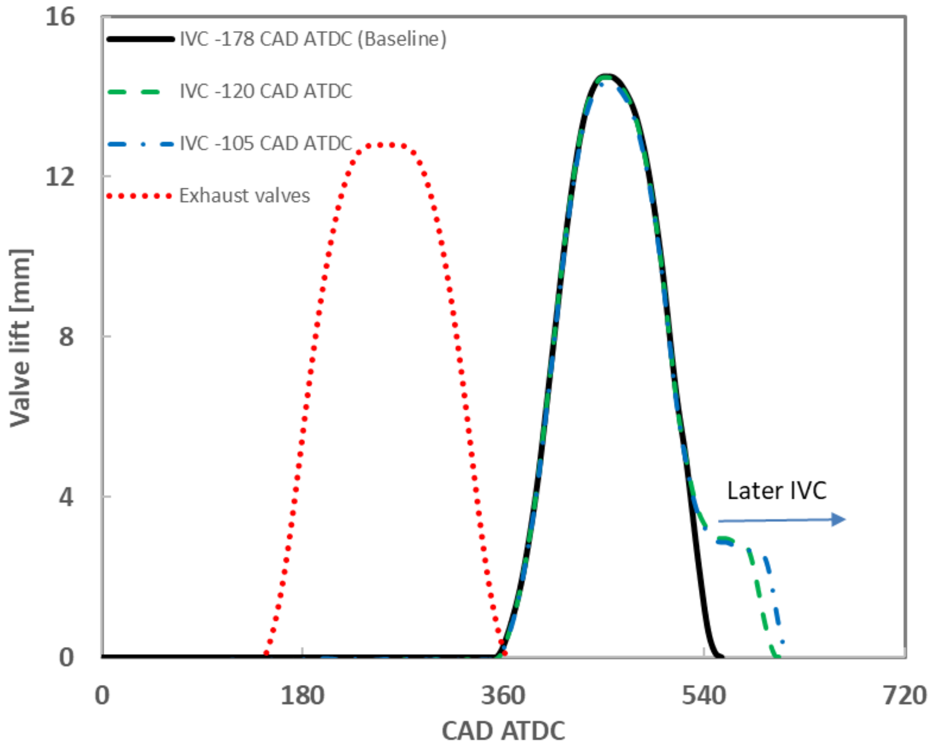

Figure 2. Fixed exhaust and variable intake valve lift profiles.

2.4 Exhaust emissions measurement

A Horiba MEXA-7170 DEGR emission analyser was used to measure the exhaust gases such as NO_x, HC, CO, and CO_2 in the exhaust pipe before the exhaust back pressure valve. In this analyser system, gases including CO and CO_2 were measured through a non-dispersive infrared absorption (NDIR) analyser, HC was measured by a flame ionization detector (FID), and NO_x was measured by a chemiluminescence detector (CLD). Specifically, the FID response was corrected by a similar method developed by Kar and Cheng [41] to account for the oxygenated organic species resultant from methanol combustion. To allow for the measurement at elevated back pressure, a high pressure sampling module was used between the exhaust sampling point and the emission analyser. A heated line was deployed to maintain the exhaust gas sample temperature of approximately 192°C to avoid condensation. The smoke number was measured downstream of the exhaust back pressure valve using an AVL 415SE Smoke Meter. The measurement was taken in filter smoke number (FSN) basis and thereafter was converted to

mg/m^3 [42]. All the exhaust gas components were converted to net indicated specific gas emissions (in g/kWh) according to [43]. In this study, the EGR rate was defined as the ratio of the measured CO_2 concentration in the intake surge tank to the CO_2 concentration in the exhaust manifold.

2.5 Data acquisition and analysis

The instantaneous in-cylinder pressure was measured by a Kistler 6125C piezo-electric pressure transducer with a sampling resolution of 0.25 CAD. The high speed and low speed National Instruments data acquisition (DAQ) cards were used to acquire the high and low frequency signals from the measurement devices. The captured data from the DAQ as well as the resulting engine parameters were displayed in real-time by an in-house developed transient combustion analysis software.

The crank angle based in-cylinder pressure traces were recorded through an AVL FI Piezo charge amplifier, averaged over 200 consecutive engine cycles, and used to calculate the IMEP and apparent heat release rate (HRR). According to [4], the apparent HRR was calculated as

$$HRR = \frac{\gamma}{(\gamma - 1)}\, p\, \frac{dV}{d\theta} + \frac{1}{(\gamma - 1)}\, V\, \frac{dp}{d\theta} \tag{4}$$

where γ is defined as the ratio of specific heats, V and p are the in-cylinder volume and pressure, respectively; and θ is the crank angle degree. Since the absolute value of the heat release is not as important to this study as the bulk shape of the curve with respect to crank angle, a constant γ of 1.33 was assumed throughout the engine cycle according to [44]. The mass fraction burned (MFB) was defined by the ratio of the integral of the HRR and the maximum cumulative heat release. Combustion phasing (CA50) was determined by the crank angle of 50% MFB. Combustion duration was represented by the period of time between the crank angles of 10% (CA10) and 90% (CA90) MFB. Ignition delay (ID) was defined as the period of time between the diesel main injection timing (SOI_main) and the start of combustion (SOC), denoted as 0.3% MFB point of the average cycle. The in-cylinder combustion stability was monitored by the coefficient of variation of the IMEP (COV_IMEP) over the sampled cycles. For the sake of simplification, the average in-cylinder gas temperature was calculated by applying the ideal gas model, considering each species in the mixture.

Net indicated efficiency (NIE) was defined as the ratio of the work done to the rate of fuel energy supplied to the engine every cycle by

$$NIE = \left[\frac{P_{ind}}{\dot{m}_{methanol}LHV_{methanol}+\dot{m}_{diesel}LHV_{diesel}}\right] * 100\% \qquad (5)$$

where P_{ind} is the net indicated power in W, $\dot{m}_{methanol}$ and $\dot{m}_{diesel}$ are the methanol and diesel mass flow rate in kg/s respectively, and LHV_{diesel} is the diesel lower heating value of 42.9×10^{6} J/kg.

The calculation of combustion efficiency was based on the unburnt exhaust products during combustion process which mainly comprised of HC and CO by

$$Combustion\ efficiency = 1 - \frac{(ISCOLHV_{CO}) + (ISHCLHV_{DF})}{\dot{m}_{methanol}LHV_{methanol} + \dot{m}_{diesel}LHV_{diesel}} * P_i \qquad (6)$$

where ISCO and ISHC are the net indicated specific emissions of CO and unburnt HC, respectively; LHV_{CO} is equivalent to 10.1×10^{6} J/kg; The energy content of the unburnt hydrocarbons was assumed to have the lower heating value of the in-cylinder fuel mixture (LHV_{DF}).

3. Methodology

3.1 Test conditions

In this study, the experimental work was carried out at a speed of 1200 rpm and a high load of 18 bar IMEP. Table 3 summarises the engine test conditions for the CDC (diesel-only) and DMDF combustion modes. The intake pressure set points of the baseline engine operation were taken from a Euro V compliant multi-cylinder HD diesel engine of the same cylinder design as the single cylinder engine. The exhaust pressures were adjusted to provide a constant pressure differential of 0.10bar above the intake pressure, in order to realize the required EGR rate and to achieve a fair comparison with equivalent pumping work.

A single diesel injection near firing TDC was used for the CDC and conventional DMDF operations. In the advanced DMDF combustion mode, however, a small amount of pre-injection fuel with an estimated volume of 3 mm^3 and a constant dwell time of 1ms (e.g. 7.2 CAD at 1200 rpm) before main diesel injection was employed to reduce the levels of PRR. The diesel main injection timings were optimised to achieve the maximum net indicated efficiency in all combustion modes. The methanol energy fraction was also varied when required. The P_{max} and PRR were limited to 180bar and 30bar/CAD, respectively. Stable engine operation was determined by controlling the COV_IMEP below 3%.

Table 3 Engine testing conditions for CDC and DMDF operations.

Parameter	Unit	CDC operation	Conventional DMDF	Advanced DMDF
Engine load (IMEP)	bar	18		
Engine speed	rpm	1200		
Diesel injection pressure	bar	1600		

Intake air pressure	kPa	260		
Exhaust back pressure	kPa	270		
Diesel injection strategy	-	Single	Single	Pre- and main injection near TDC
Diesel SOI_main	CAD ATDC	Swept	Swept	Swept
Intake air temperature	℃	50	50	Swept
MF	%	0	Swept	Swept
EGR rate	%	0	0	Swept
Effective compression ratio	-	16.8	16.8	Swept

4. Results and discussion

4.1 The effect of methanol energy fraction

Figure 3 shows the in-cylinder pressure and HRR while Figure 4 shows the average in-cylinder gas temperatures for the high load DMDF operation. The diesel SOI is an important factor in maximizing engine efficiency and curbing emissions. In order to achieve high net indicated efficiency, the SOI was swept for different combustion control strategies. In this study, single diesel injection timing was used in a conventional DMDF engine and optimised to achieve the maximum engine thermal efficiency with different methanol energy fractions varying from 0% (diesel-only) to the maximum value of 28% limited by the peak cylinder pressure or heat release rate.

Figure 3 and Figure 4 show that an increase in the methanol energy fraction resulted in lower in-cylinder compressed gas pressure and temperature. This was mainly attributed to the two following reasons. Firstly, a higher MF increased the total in-cylinder mass trapped. This was attributed to the relatively lower LHV of methanol than the diesel fuel, which required more methanol volume fraction to maintain the same engine output. Secondly, the cooling effect achieved with higher MF due to the high latent heat of vaporization of the methanol [45]. The charge cooling effect helped to decrease the charge temperature at the end of compression by up to 42 K. However, it was observed that the PRR and P_{max} increased very rapidly with higher MF to exceed their limits of 180bar and 30bar/CAD if the SOI was kept constant, because of the greater heat release of the increased premixed methanol charge. Therefore, the diesel injection timing had to be retarded from -8 CAD ATDC to -3 CAD ATDC with higher MF in order to keep the PRR and P_{max} below their limits. It can be also seen from Figure 3 that the maximum MF tends to be limited by the PRR rather than P_{max} at a higher MF condition, as suggested by the lower P_{max} of the optimised DMDF operation with MF of 28%.

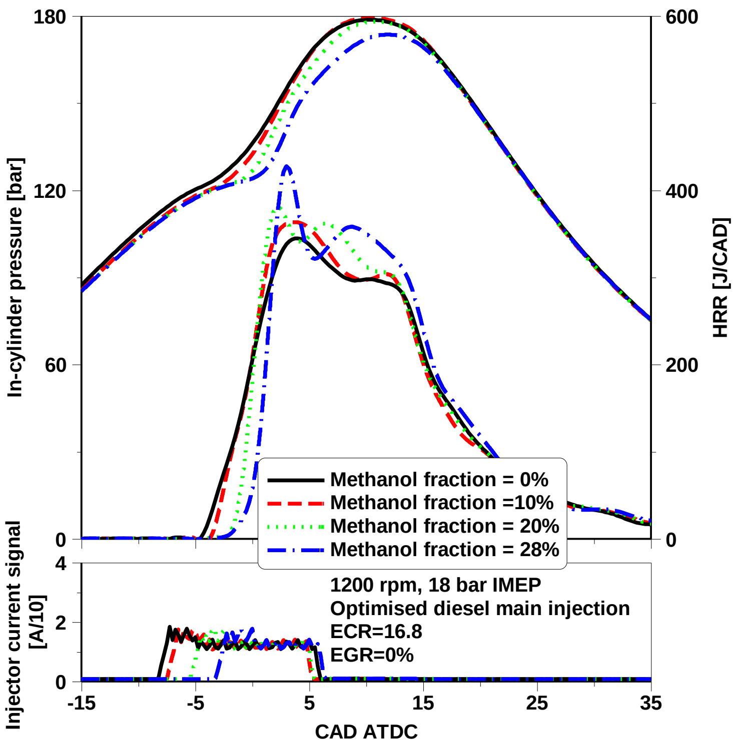

Figure 3. In-cylinder pressure, HRR, and diesel injector signal for optimised high load DMDF operation with different MF.

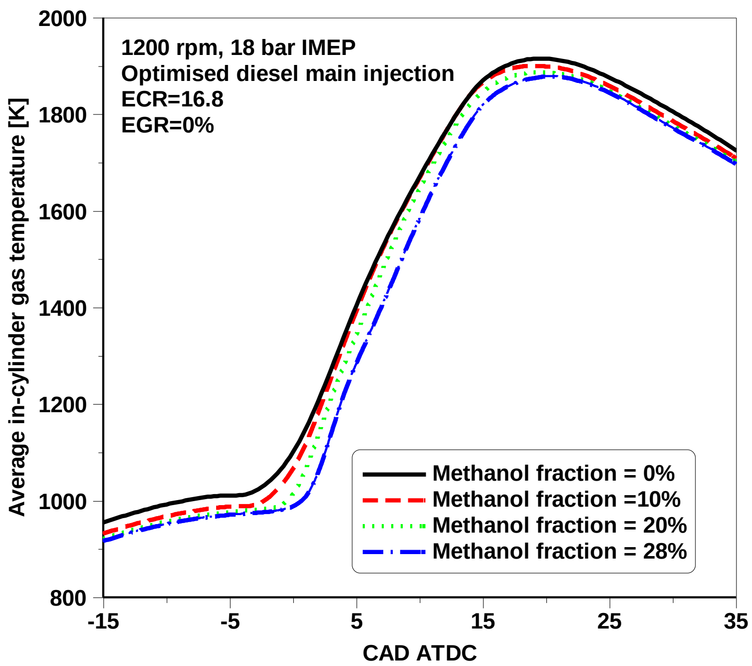

Figure 4. Average in-cylinder gas temperature for optimised high load DMDF operation with different MF.

As the SOI was delayed towards TDC with increased MF, the ignition delay was reduced due to higher charge temperatures as shown in Table 4, which shows the combustion characteristics, performance, and emissions of the CDC and conventional DMDF operation with different methanol energy fractions. A higher COV_IMEP was observed likely due to the higher peak heat release and lower local combustion temperature. The delayed combustion process as well as lower charge temperature prior to combustion decreased the average combustion gas temperature, resulting in lower NO_x emissions. The shorter ignition delay caused more diffusion burn of diesel and hence slightly higher soot emissions. The increase in the CO and HC emissions were possibly a result of more premixed fuel trapped in the crevice and squish volumes as well as more diffusion combustion of diesel and lower in-cylinder combustion temperature, yielding lower combustion efficiencies as reported in [46]. However, the reduction in heat transfer losses due to lower in-cylinder combustion temperature offset the adverse effect caused by the decreased combustion efficiency as the MF was increased from 0 to 20%, resulting in a higher net indicated efficiency. When the MF was further increased to 28%, however, the improvement in heat loss was weakened as more combustion was taken place in the expansion stroke. Additionally, the combustion efficiency was further decreased. These effects resulted in a lower net indicated efficiency when operating DMDF with MF of 28% than MF of 20%.

Table4. The effect of MF on optimised high load conventional DMDF operation with single diesel injection.

Parameter	Unit	MF=0%	MF=10%	MF=20%	MF=28%
Diesel SOI	CAD ATDC	-8	-7.25	-5.25	-3
COV_IMEP	%	0.40	0.54	1.08	1.67
PRR	bar/CAD	19.2	24.5	28.4	29.6
P_{max}	bar	180.1	179.5	179.0	174.4

Ignition delay (SOC-SOI)	CAD	5.0	4.6	3	0.75
CA50	CAD ATDC	9.0	8.8	9.0	10.0
CA10-CA90	CAD	21.5	21.3	20.9	20.4
Lambda	-	1.98	2.04	2.09	2.11
ISsoot	g/kWh	0.0013	0.0015	0.0017	0.0018
$ISNO_x$	g/kWh	17.5	16.5	14.3	12.7
ISCO	g/kWh	0.1	1.4	2.9	3.6
ISHC	g/kWh	0.13	0.45	0.99	1.54
Combustion efficiency	%	99.9	99.5	99.0	98.6
NIE	%	45.3	45.7	46.1	45.79

4.2 The effect of EGR

Following the studies on the conventional DMDF combustion with a single diesel injection, the pilot injection was introduced and found to be effective to reduce PRR and P_{max}, as can be seen in the results of 28% MF in Tables 3 and 4. The pilot injection was kept constant at 3 mm^3 with a constant dwell time of 1ms. This section presents the experimental results in terms of the effect of EGR on the optimised DMDF combustion with the pilot injection. The boundary conditions were held constant and the MF was maintained at 28%. Figure 5 shows the in-cylinder pressure, diesel injection, and HRR curves of the optimum DMDF operation at 0% and 17% EGR. The decreased oxygen concentration and increased heat capacity of the in-cylinder charge with the use of EGR increased the main injection delay, allowing for a more advanced diesel SOI_main to optimise the engine efficiency. It can be seen that there was a small heat release of the pre-injected diesel occurred prior to the main diesel injection in both operations with and without EGR. With EGR the ignition delays for both pilot injection and main diesel injection were slightly longer than those without EGR, resulting in the slightly higher percentage of premixed combustion in the first heat release peak with EGR.

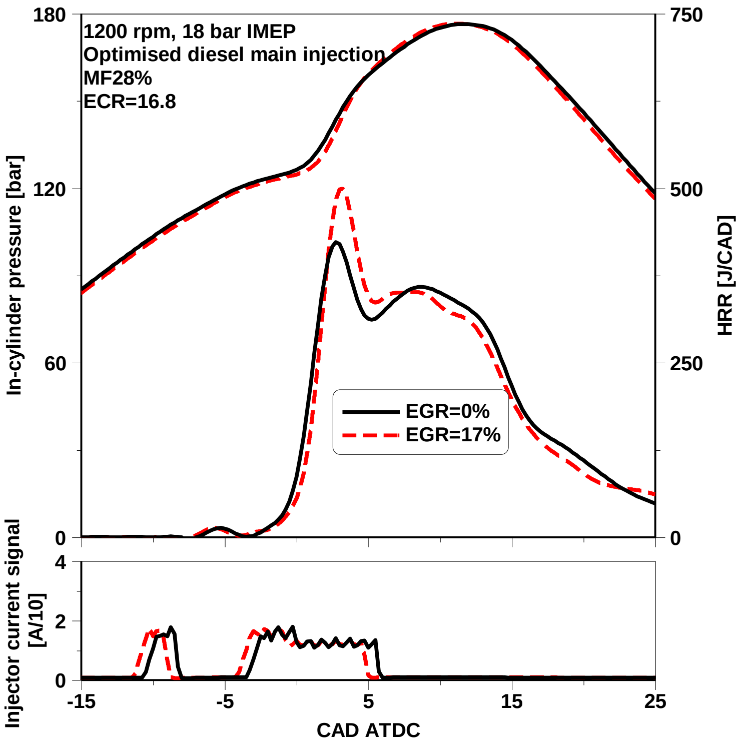

Figure 5. In-cylinder pressure, HRR, and diesel injector signal for optimised high load DMDF operation with and without EGR.

Table 5 summarises the resulting performance and emissions results of the optimised DMDF operation with and without EGR. The addition of EGR delayed the combustion process and increased the combustion duration, despite the CA50 was maintained similar to the case without EGR by an advanced diesel SOI_main. The NO_x emissions were drastically reduced from 12.9 to 4.4 g/kWh while the soot emissions were slightly increased due to the lower combustion temperature and a reduction in in-cylinder lambda. The longer mixing period and lower lambda contributed to a small decrease in CO and HC emissions and thus slightly higher combustion efficiency. Net indicated efficiency with EGR was higher than that without EGR, which possibly was a result of higher peak heat release, slightly higher combustion efficiency, and lower combustion temperature.

Table5. The effect of EGR on optimised high load DMDF operation with pilot injection.

Parameter	Unit	EGR=0%	EGR=17%
MF	%	28	28
Diesel SOI_main	CAD ATDC	-3.25	-4.0
COV_IMEP	%	1.66	1.60
PRR	bar/CAD	23.5	24.1
P_{max}	bar	178	178
Ignition Delay (main)	CAD	0.75	1.6
CA50	CAD ATDC	9.5	9.3
CA10-CA90	CAD	20.1	21.8
Lambda	-	2.1	1.7
ISsoot	g/kWh	0.0013	0.0019
$ISNO_x$	g/kWh	12.9	4.4
ISCO	g/kWh	3.6	3.4
ISHC	g/kWh	1.6	1.3
Combustion efficiency	%	98.5	98.9
NIE	%	46.15	46.57

4.3 The effect of Miller cycle

The Miller cycle was employed in this section in an attempt to minimise the PRR and the in-cylinder pressure to enable a more advanced combustion phasing for improving upon engine efficiency. Figure 6 depicts the effect of DMDF operation with different ECR on the heat release characteristics. The methanol energy fraction was maintained at 28% and the diesel main injection timings were optimised up to the PRR or peak in-cylinder pressure limitations.

The decreased ECR via LIVC effectively reduced the compressed gas pressure and temperature before combustion as shown in Figure 7. This successfully delayed the ignition and combustion of the premixed fuel and thus suppressed the PRR and P_{max}, allowing for a much more advanced diesel SOI_main to optimise the engine efficiency. The two distinct heat release events in the baseline ECR of 16.8 disappeared when operating with a lower ECR. This was a result of the increased mixing period during the ignition period and thus a more homogeneous combustion as supported by the significantly higher peak heat release. A reduction in ECR led to higher average in-cylinder gas temperature during combustion attributed to a decrease in the in-cylinder mass trapped and therefore decreased the total heat capacity of gases. The reason for the slightly lower P_{max} in the ECR of 14.3 was due to the high level of PRR, which limited the optimisation of diesel injection timing. It is noted that a small amount of heat release from the pre-injected diesel occurred before diesel SOI_main at the ECR of 16.8 was successfully prevented by lowering the ECR. This was a result of the decreased compressed gas temperature, which avoid the heat release of the premixed charge.

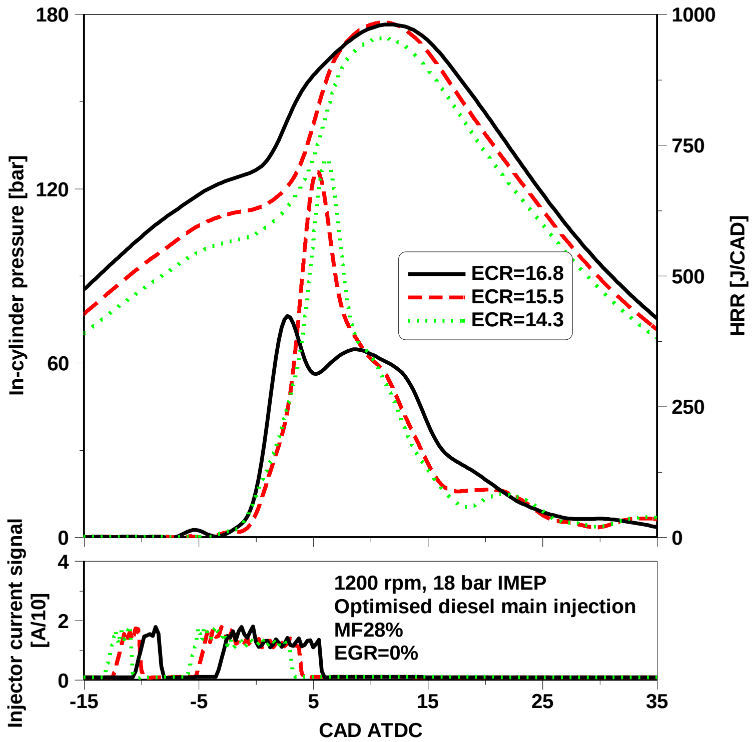

Figure 6. In-cylinder pressure, HRR, and diesel injector signal for optimised high load DMDF operation with different ECR.

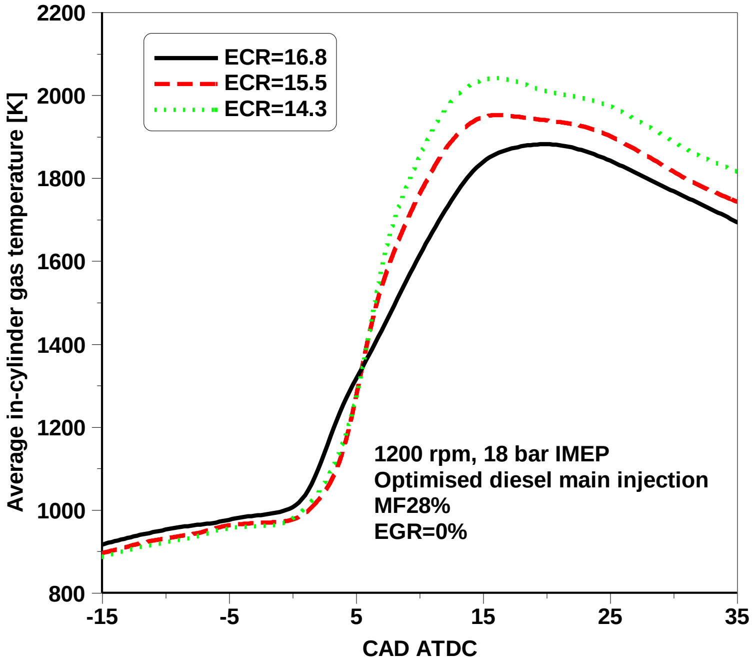

Figure 7. Average in-cylinder gas temperature for optimised high load DMDF operation with different ECR.

Table 6 shows the resulting combustion characteristics, performance, and emissions of the optimised DMDF operation with different ECR. As the ECR decreased, the optimum diesel main injection was advanced. This resulted in an increase in PRR while had less impact on combustion characteristics and engine emissions. Additionally, the lower ECR slightly improved the combustion efficiency, which along with the resulting faster HRR contributed to the improvement in engine thermal efficiency.

Table 6. The effect of EGR on optimised high load DMDF operation.

Parameter	Unit	ECR=16.8	ECR=15.5	ECR=14.3
MF	%	28	28	28
Diesel SOI_main	CAD ATDC	-3.25	-5	-5.75

Ignition Delay (main)	CAD	0.75	3.3	3.9
COV_IMEP	%	1.66	1.46	1.66
PRR	bar/CAD	23.5	28.5	29.4
P_{max}	bar	178	178.5	174
CA50	CAD ATDC	9.5	8.0	8.0
CA10-CA90	CAD	20.1	19.0	20.2
Lambda	-	2.1	1.9	1.7
ISsoot	g/kWh	0.0013	0.0010	0.0012
$ISNO_x$	g/kWh	12.9	13.3	12.2
ISCO	g/kWh	3.6	3.1	2.7
ISHC	g/kWh	1.6	1.2	2.7
Combustion efficiency	%	98.5	98.9	99.2
NIE	%	46.15	46.23	46.41

4.4 The effect of intake air cooling

The last approach used in this study to control the PRR and P_{max} of the DMDF combustion is the intake air cooling. The experiments were performed without EGR at the baseline ECR of 16.8. The diesel injection timings were optimised and the MF was maintained at 28%. The intake air temperature (T_{int}) was controlled by using an air-to-water cooler and an intake air heater.

Figure 8 shows the in-cylinder pressure, diesel injection, and HRR curves of the optimised DMDF operation with a pilot injection at different intake air temperatures. A reduction in the T_{int} from 323 to 305 K effectively decreased the average in-cylinder gas temperature by 50 K during the compression process, as demonstrated in Figure 9. Therefore, the ignition delay of the premixed charge was increased to allow for an advanced diesel SOI_main to be used. The decreased compressed gas temperature also prevented the autoignition and heat release of the premixed fuel prior to the diesel SOI_main. The in-cylinder gas pressure during compression stroke was similar to that with higher T_{int} of 323 K due to the balance effect between the lower compressed gas temperature and the resulting higher in-cylinder gas density. The longer mixing period noticeably increased the peak heat release while the delayed combustion process and decreased compressed gas temperature contributed to a reduction in the average in-cylinder gas temperature during the combustion process.

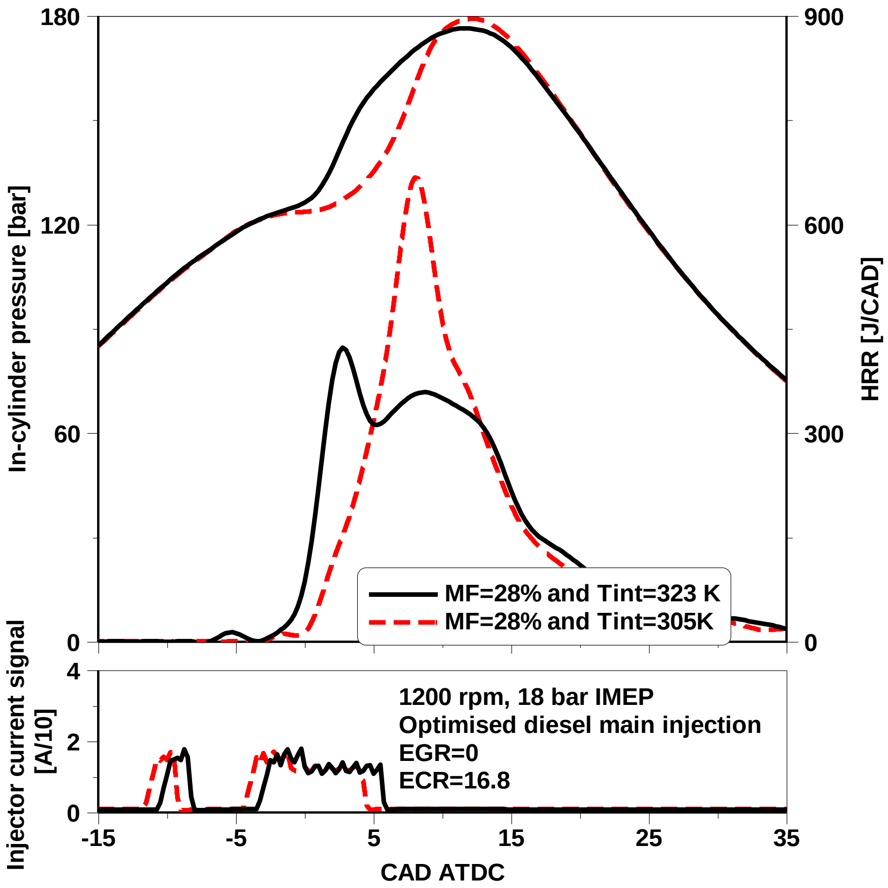

Figure 8. In-cylinder pressure, HRR, and diesel injector signal for optimised high load DMDF operation with different T_{int} and MF.

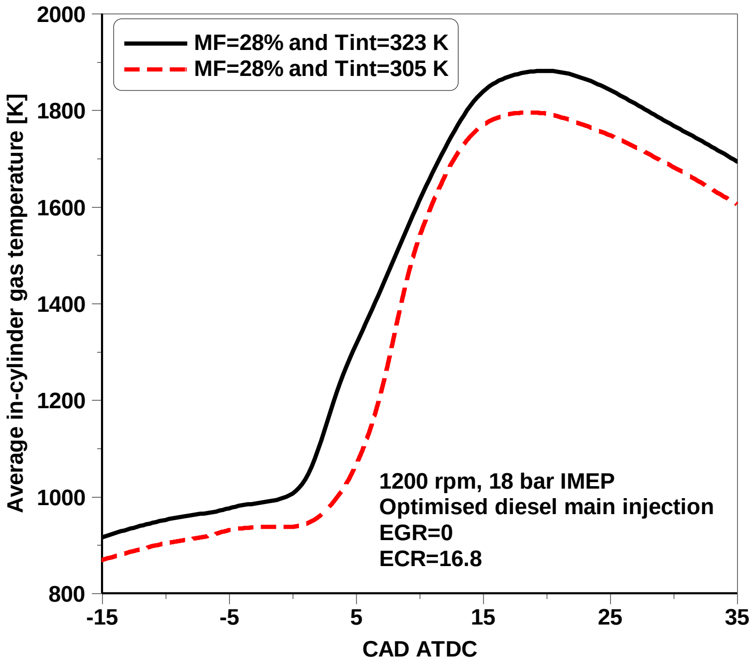

Figure 9. Average in-cylinder gas temperature for optimised high load DMDF operation with different T_{int} and MF.

The combustion characteristics, performance and emissions results of the optimised DMDF operation with different intake coolant temperatures are summerised in Table 7. Compared to the higher T_{int}, the DMDF operation with a lower T_{int} advanced the optimum diesel main injection timing while reducing the level of PRR. The reduction in T_{int} with optimised diesel main injection timing produced slight impact the combustion characteristics and emissions. The resulting higher degree of premixed combustion and lower average in-cylinder gas temperature promoted the engine thermal efficiency from 46.15% to 47.05%.

Table7. The effect of EGR on optimised high load DMDF operation.

Parameter	Unit	T_{int}=323K	T_{int}=305K
MF	%	28	28
Diesel SOI_main	CAD ATDC	-3.25	-4.25
Ignition Delay (main)	CAD	0.75	4.1

COV_IMEP	%	1.66	1.84
PRR	bar/CAD	23.5	18.9
P_{max}	bar	178	180
CA50	CAD ATDC	9.5	9.6
CA10-CA90	CAD	20.1	18.1
Lambda	-	2.1	2.2
ISsoot	g/kWh	0.0013	0.0014
$ISNO_x$	g/kWh	12.9	12.7
ISCO	g/kWh	3.6	5.3
ISHC	g/kWh	1.6	1.9
Combustion efficiency	%	98.5	98.2
NIE	%	46.15	47.05

4.5 Analysis of DMDF operation with combined Miller cycle and intake air cooling

This subsection aims to analyse the effect of the DMDF operation with both Miller cycle and intake air cooling on combustion process and explore their potential for increasing the maximum net indicated efficiency. A pre-injection with an estimated volume of 3 mm^3 and a constant dwell time of 7.2 CAD to the diesel main injection was introduced. The diesel injection timings were adjusted for engine operations with ECR of 16.8 and 14.3 and methanol energy fractions of 28% and 40%. The operation with a limited MF of 28% at an ECR of 16.8 and T_{int} of 323 K was taken as the reference and no EGR was used.

4.5.1 Combustion characteristics of DMDF operation with Miller cycle and intake air cooling

Figure 10 shows the in-cylinder pressure, diesel injection, and HRR curves of the different optimised DMDF combustion modes. A higher MF of 40% can be obtained when applying Miller cycle or intake air cooling strategies. Figure 11 depicts that the use of Miller cycle and lower T_{int} with a higher MF effectively decreased the average in-cylinder gas temperature during compression stroke, reducing up to nearly 90 K in their combination when compared to the baseline operation. This substantially delayed the ignition timing of the premixed charge and potentially minimised the PRR and P_{max}, allowing for a more advanced diesel injection timing to improve upon the engine efficiency. As a consequence, the longer premixed period and relatively higher MF significantly increased the peak heat release. The compressed gas pressure was decreased by the lower ECR, which was not achievable by the use of a lower T_{int}. This was primarily attributed to the increased in-cylinder gas density, as to be demonstrated in the later part of this section. A relatively lower peak in-cylinder pressure observed in the operation with MF of 40% at an ECR of 14.3 and T_{int} of 323 K was because the main diesel injection timing was limited by higher levels of the PRR. Moreover, the average in-cylinder gas temperature during combustion process was increased in the lower ECR cases due to the lower in-cylinder mass trapped while was decreased in the lower T_{int} at an ECR of 16.8, which was attributed to the higher in-cylinder charge mass and lower compressed gas temperature.

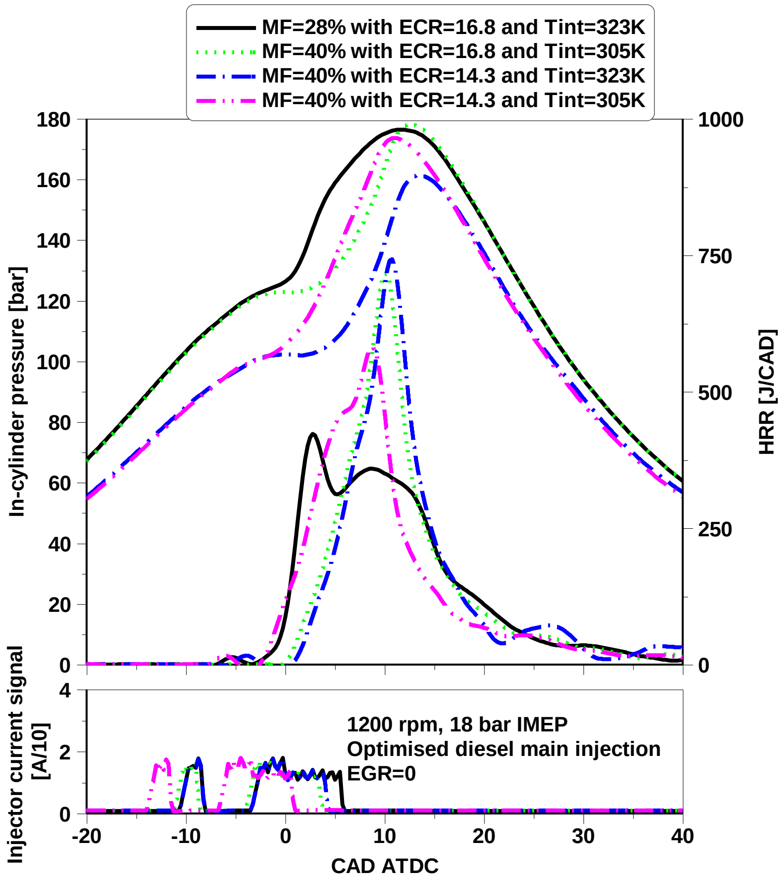

Figure 10. In-cylinder pressure, HRR, and diesel injector signal for optimised high load DMDF operation with Miller cycle and intake air cooling.

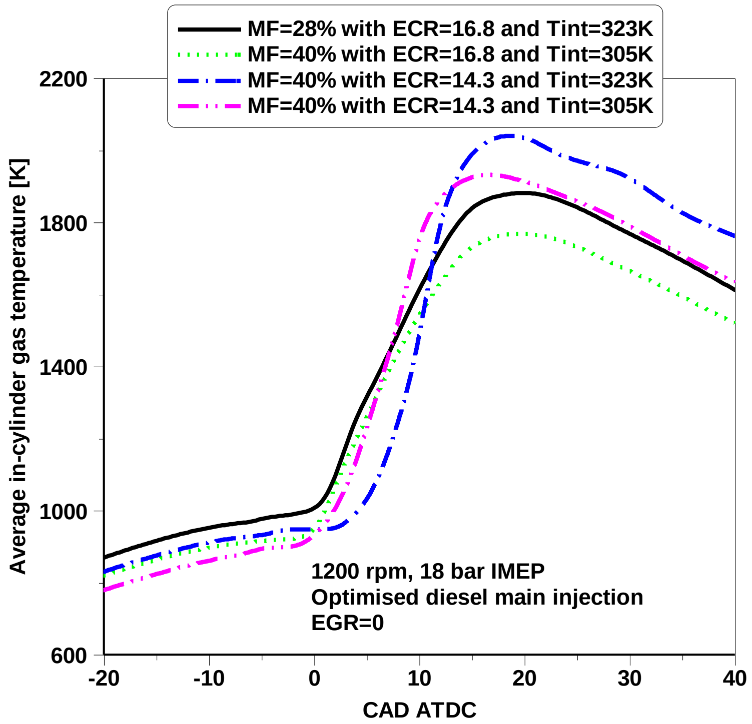

Figure 11. Average in-cylinder gas temperature for optimised high load DMDF operation with Miller cycle and intake air cooling.

Figure 12 shows the combustion characteristics as a function of the diesel SOI_main for different DMDF combustion modes. For a constant diesel SOI_main with MF of 40%, the CA50 (e.g. combustion phasing) was delayed by a lower ECR and T_{int} because of the delayed combustion process. However, much earlier diesel SOI_main enabled by the combined lower ECR and lower T_{int} advanced the combustion process. The higher degree of premixed combustion with the use of lower ECR and lower T_{int} accelerated the initial combustion, as evidenced by a shorter period of CA10-CA50 than that of the baseline operation. On the contrary, the weakened mixing-control combustion lengthened the late combustion process as measured by a longer period of CA50-CA90. As a consequence, the period of CA10-CA90 (e.g. combustion duration) for the DMDF operation with 40% MF was shortened when diesel SOI_main was optimised for the lower ECR or lower T_{int}. As shown in Figure 10, however, the combustion duration was longer if the diesel SOI_main was kept constant when the ECR or/and T_{int} were decreased. This was mainly attributed to the slower mixing-controlled combustion, which was supported by the decreased heat release of the late combustion phase.

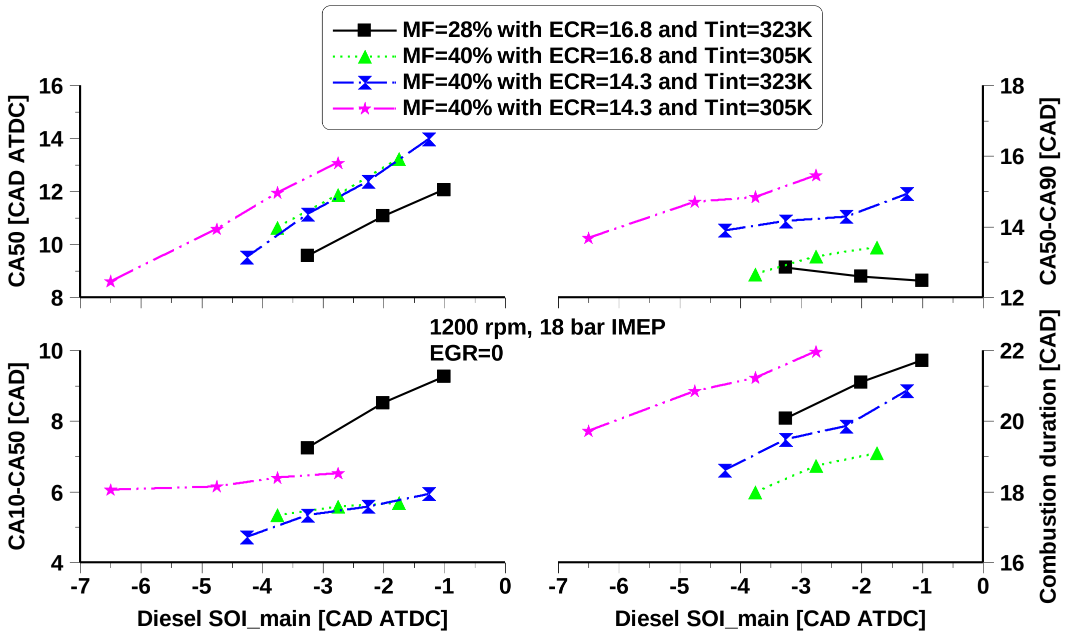

Figure 12. Combustion characteristics for optimised high load DMDF operation with Miller cycle and intake air cooling.

4.5.2 Exhaust emissions and performance of DMDF operation with Miller cycle and intake air cooling

Figure 13 and Figure 14 depict the net indicated specific emissions and engine performance versus the diesel SOI_main respectively for the different combustion modes. The DMDF operation with higher MF at a lower ECR and T_{int} achieved a significant reduction in NO_x emissions. This was likely a result of the more homogeneous combustion as less diesel fuel was burned during the mixing-controlled combustion process and the lower compressed gas temperature caused by Miller cycle and intake air cooling, which led to a lower peak combustion temperature. In particular, the cases with Miller cycle yielded lower NO_x emissions, which associated with the lower in-cylinder lambda as demonstrated in Figure 14. Miller cycle, intake cooling, and a higher MF produced little impact on the soot emissions. All soot emissions were below 0.002 g/kWh, which was well below than the Euro VI particulate matter limit of 0.01 g/kWh even without the diesel particulate filter [47].

The CO and HC emissions were substantially increased as more methanol was injected at a lower T_{int} of 305 K. This phenomenon was likely attributed to the increased premixed methanol-air mixture trapped in the squish and crevice regions as reported in [19,46]. Additionally, the decreased in-cylinder gas temperature was also play an important role on the increase in HC and CO emissions. As a result, the combustion efficiency was reduced. The use of Miller cycle helped to suppress the HC and CO emissions, especially when operating at a higher T_{int} of 323 K. This was possibly a result of the lower in-cylinder compression pressure, which minimised the amount of premixed fuel pressed into the squish and crevice regions. Apart from that, the faster HRR and higher in-cylinder fuel-air ratio increased the mean in-cylinder gas temperatures during combustion, which probably was one of the reasons for a reduction in HC and CO emissions as it could help to improve the oxidation of HC and CO emissions [48]. Consequently, this allowed for higher combustion efficiency than those achieved with reference case.

The use of Miller cycle and intake air cooling at a higher MF decreased the levels of PRR, which was linked to the reduction in compression temperatures. Figure 14 also revealed that a reduction in the T_{int} increased the net indicated efficiency at the optimised diesel SOI_main, especially when combining with Miller cycle. This was likely a result of more homogeneous combustion and lower heat transfer losses resulted from the lower local combustion temperature. However, the use of Miller cycle with MF of 40% at a higher T_{int} slightly decreased the net indicated efficiency despite a small increase in combustion efficiency. This was possibly due to the decreased in-cylinder lambda and a higher average in-cylinder gas temperature during combustion, which could increase the heat losses.

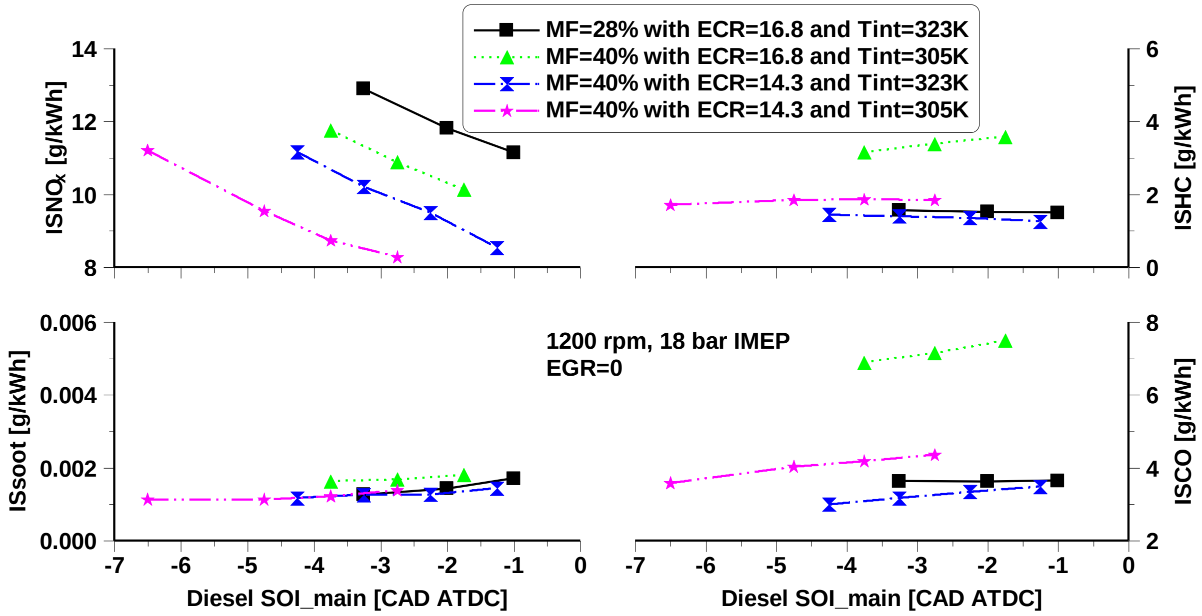

Figure 13. Net indicated specific emissions for optimised high load DMDF operation with Miller cycle and intake air cooling.

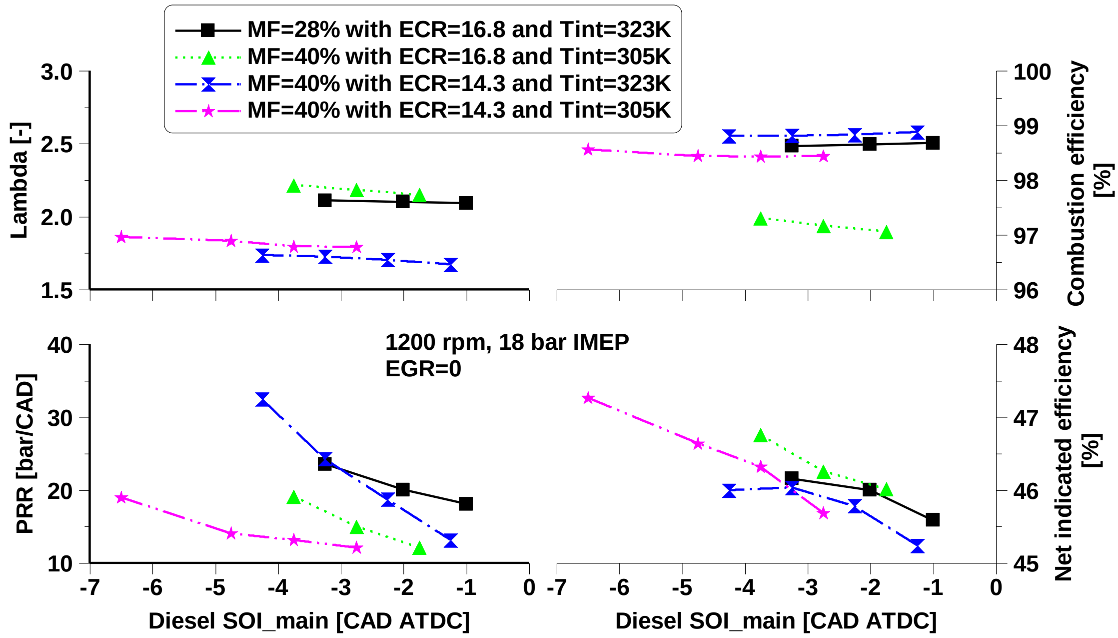

Figure 14. Engine performance for optimised high load DMDF operation with Miller cycle and intake air cooling.

4.6 Comparison of different engine combustion modes

This subsection performs a comparison of the different combustion modes in terms of combustion characteristics, engine-out emissions, and performance, in order to explore advanced combustion control strategies for efficient high load DMDF operation.

Figure 15 shows the optimised diesel SOI_main and combustion characteristics for the CDC (e.g. black bar) and DMDF operation with lower MF of 28% at higher T_{int} of 323 K (e.g. red bar) and with higher MF of 40% at lower T_{int} conditions (e.g. green bar). It should be note that the use of recycled exhaust gas limited the lowest intake air temperature to 310 K when operating with an EGR rate of 17%. Compared to the CDC, the optimised diesel SOI_main was delayed in the DMDF operation in order to avoid excessive PRR and peak in-cylinder pressure limit. This delayed the CA50 and CA90, but the period of CA10-CA90 was decreased due to a more homogeneous combustion than that of the CDC. The use of EGR and Miller cycle enabled an earlier diesel injection timing, which helped to advance the CA50. However, the DMDF operation with EGR at a higher T_{int} lengthened the mixing-control combustion as measured by a later CA90. This was the reason for a longer period of CA10-CA90. At a lower T_{int}, however, the DMDF operation with EGR achieved shorter period of CA10-CA90 than those attained without EGR. This phenomenon was possibly linked to the relatively higher T_{int} by 5 K when operating with EGR of 17%, which accelerated the combustion process. Overall, the DMDF operation with higher MF at a lower T_{int} allowed for relatively advanced diesel injection timing and shorter CA10-CA90 than those with a lower MF at a higher T_{int}.

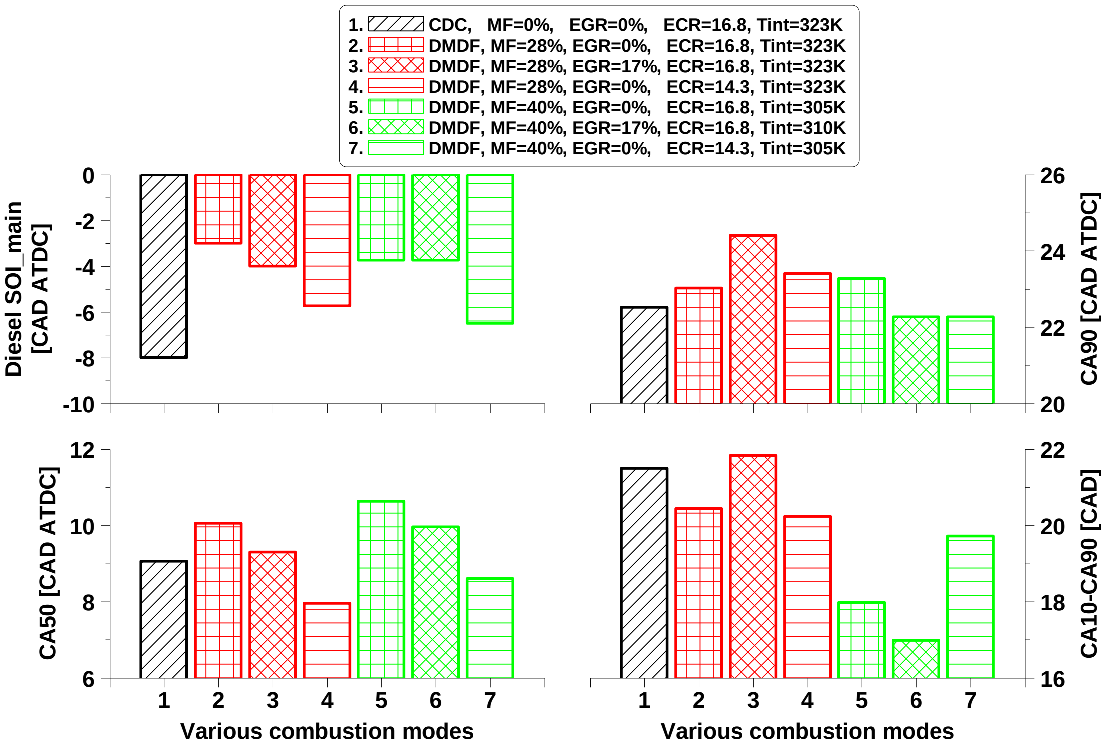

Figure 15. Comparison of main diesel injection timing and combustion characteristics for optimised CDC and DMDF operations.

Figure 16 depicts the net indicated specific emissions for the most efficient cases in different combustion modes. The DMDF operation achieved lower NO_x emissions than the CDC, reducing NOx emissions from 17.5 g/kWh in the CDC operation to12.7 g/kWh in the DMDF operation with MF of 28%. The use of EGR decreased the in-cylinder oxygen availability and increased the total gas heat capacity, yielding further significantly lower NO_x emissions. As a result, the introduction of EGR decreased NO_x emissions from 12.7 to 4.4 g/kWh and 11.7 to 4.1 g/kWh (e.g. 65% reduction) under DMDF operation with MF of 28% and 40%, respectively. Additionally, the optimised DMDF operation with Miller cycle and intake air cooling obtained a slight reduction in NO_x emissions to 11.2 g/kWh. The variations in soot emissions were insignificant in all combustion modes, maintaining a very low level of less than 0.002 g/kWh, which is well below Euro VI particulate matter limit even without the diesel particulate filter. However, the DMDF operation apparently increased the CO and HC emissions, which was a result of the occurrence of the premixed fuel trapped in the squish and crevice volumes. Particularly when operating with a higher MF at a lower intake air temperature, the CO and HC emissions were much higher. The lower average in-cylinder gas temperature during combustion also contributed to an increase in the CO and HC emissions. It can be also seen that the use of Miller cycle helped to minimise the CO and HC emissions due to the increased combustion temperature.

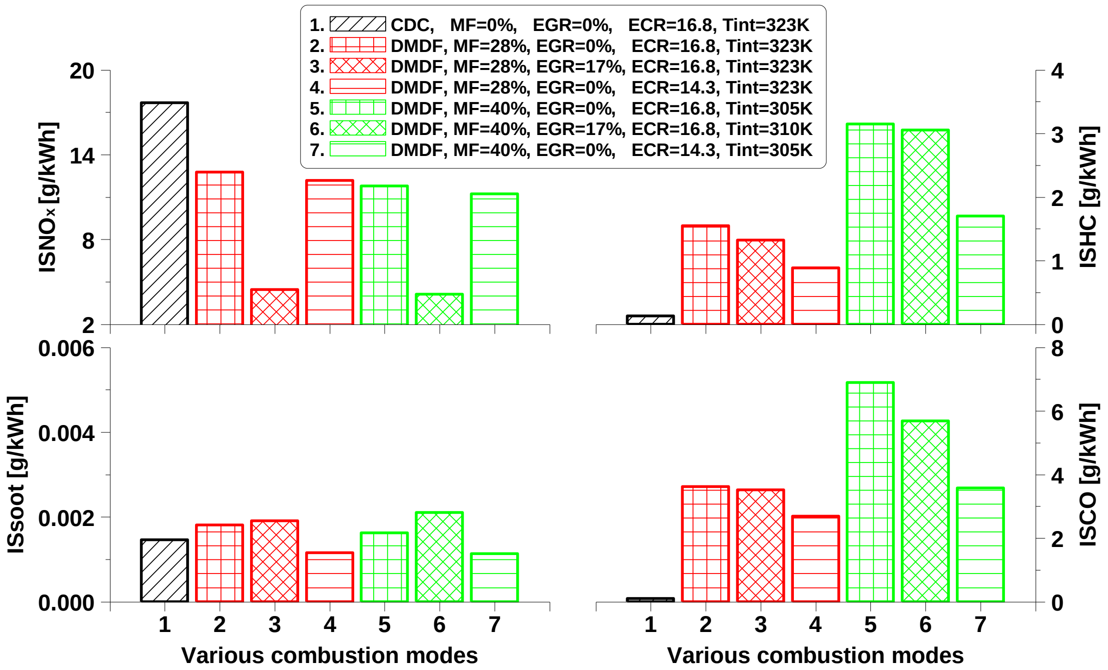

Figure 16. Comparison of Net indicated specific emissions for optimised CDC and DMDF operations.

Figure 17 depicts a comparison of engine performance between the CDC and DMDF operation with lower MF at a higher T_{int} and with a higher MF at a lower T_{int} conditions, respectively. The baseline DMDF operation at an ECR of 16.8 without EGR increased the in-cylinder lambda compared to the CDC. The application of Miller cycle and EGR clearly decreased the in-cylinder lambda. A reduction in the T_{int} substantially decreased the levels of PRR compared to those with higher T_{int} at the most efficient cases. This also revealed that the limitation for the improvement in engine efficiency was the P_{max} rather than the PRR when operating the high load DMDF with intake air cooling. It can be also seen that the PRR of the DMDF operation with EGR at a higher T_{int} was relatively lower. This was due to the later optimised diesel SOI_main, which was constrained by the P_{max}. However, the PRR was relatively higher when the DMDF operation with EGR at a lower T_{int} condition. This was a result of the relatively higher T_{int} by 5 K when introducing the recycled exhaust gas, which advanced the ignition timing of the premixed charge.

The increased HC and CO emissions in the DMDF operation (as shown in Figure 16) was the reason for the decrease in the combustion efficiency, particularly at a higher MF and lower intake air temperature. The DMDF operation obtained higher net indicated efficiency than the CDC due to more homogeneous combustion with lower heat transfer losses. This was become more obvious at the lower T_{int}. There were also exceptions when operating DMDF with EGR at the lower T_{int}, the net indicated efficiency was much lower possibly linked to the relatively higher T_{int} of 310 K. The leaner DMDF operation with MF of 40% at an ECR of 14.3 and T_{int} of 305 K allowed for more advanced CA50 and higher peak heat release. Therefore, the net indicated efficiency was increased from 45.7% of the CDC and 46.2% of the DMDF with 28% MF to the highest of 47.4% of the optimised DMDF with a higher MF of 40% and lower ECR without EGR. Although the DMDF operation with EGR can potentially achieve low levels of NO_x emissions, the use of recycled exhaust gas limited the intake air temperature control, which inhibited the improvement in the net indicated efficiency (46.0%).

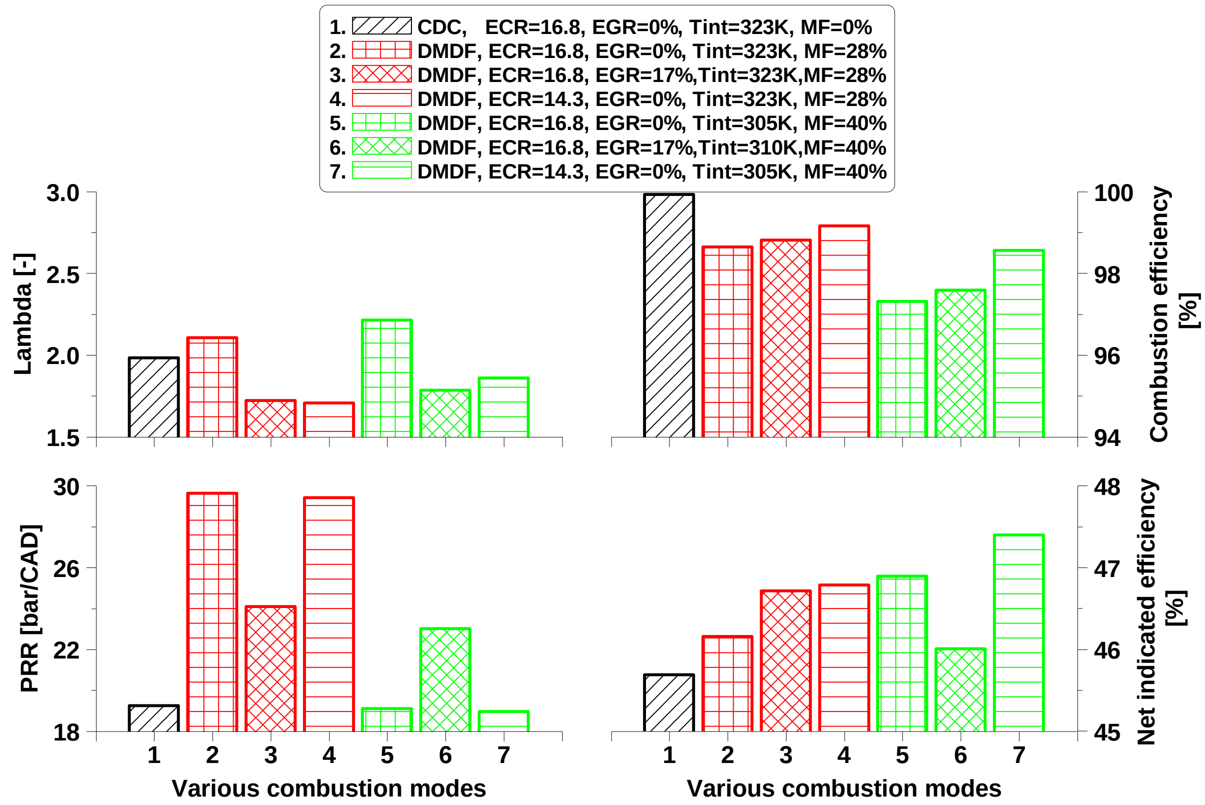

Figure 17. Comparison of engine performance for optimised CDC and DMDF operations.

5. Conclusions

In this study, systematic experiments were performed on a heavy-duty diesel engine operating at a high engine load of 18 bar IMEP with the aim to improve the high load diesel-methanol dual-fuel operation in terms of the percentage of methanol as well as the engine performance and emissions. Miller cycle, EGR, and intake air cooling achieved were investigated as effective combustion control strategies for extending the DMDF operation with higher methanol energy fraction and increasing the net indicated efficiency. The effect of the Miller cycle combined with lower intake air temperature on the combustion characteristics, exhaust emissions, and performance of the DMDF operation was also analysed. Finally, a comparison of the different combustion control strategies for the DMDF operation was performed to quantify their potential benefit compared to the conventional diesel combustion. The primary findings can be summarised as follows:

1. In the high load engine operation, a higher level of pressure rise rate was observed as the methanol energy fraction was increased. As such, the limitation for engine efficiency improvement was transferred from the P_{max} encountered in the CDC to the PRR in the DMDF combustion. This was a result of a faster and more homogeneous combustion occurred in the DMDF combustion with a limited MF to 28%.
2. The introduction of EGR of 17% demonstrated very little impact on the ignition timing of the premixed charge as evidenced by the existence of the two distinct heat release events. This was likely attributed to the insignificant impact on the in-cylinder gas temperature during compression.
3. The application of Miller cycle via LIVC and the reduction in intake air temperature via an air-to-water heat exchanger demonstrated the potential for higher methanol substitution ratios as it apparently decreased the in-cylinder gas temperature during compression. This successfully delayed the ignition timing of the premixed charge and thus decreased the levels of PRR and P_{max}, allowing for a better combustion control.
4. The combination of Miller cycle and intake air cooling effectively improved the DMDF operation to a higher MF of 40% by keeping PRR below the limit through the optimised diesel injection timing. The resulting more homogeneous combustion and lower heat transfer losses resulted from the lower local combustion temperature decreased the NO_x emissions and increased the net indicated efficiency.
5. The high load DMDF combustion decreased the average in-cylinder gas temperature, allowing for a reduction in heat transfer loss at the expense of lower combustion efficiency when compared to the CDC. Consequently, the overall engine efficiency was the

counterbalance result between the improvement in heat transfer losses and the penalty in combustion efficiency.

6. The optimised DMDF combustion attained higher net indicated efficiency than the CDC. This improvement became more obvious when operating at a lower intake air temperature despite lower combustion efficiency. The lower T_{int} also helped to minimise the levels of PRR in the optimised DMDF operation with or without using Miller cycle or EGR when compared to those at higher T_{int}.
7. Optimised DMDF operation with EGR of 17% and MF of 40% at a lower T_{int} condition achieved the lowest NO_x emissions of 4.1 g/kWh. However, the improvement in thermal efficiency was inhibited by the intake air temperature control as the use of recycled exhaust gas limited the intake air temperature to 310 K.
8. Preferably, the optimised DMDF operation with Miller cycle (e.g. ECR=14.3) and MF of 40% at a lower T_{int} attained the highest net indicated efficiency of 47.4%, which was increased by 3.7% and 2.6% respectively when compared to the optimised CDC (45.7%) and conventional DMDF (46.2%). This improvement was accompanied with a reduction of 37% in NO_x emissions and little impact on soot emissions in comparison with the CDC.

Overall, this work evidences the ignition timing of the premixed methanol is closely related to the compression temperature and demonstrates the potential of Miller cycle and intake air cooling as effective combustion control strategies for in-cylinder gas temperature control and thus to achieve efficient high load DMDF operation with the greater use of methanol.

Contact information

Dr Wei Guan

Email: gwei916@163.com

or

Professor Hua Zhao

Email: hua.zhao@brunel.ac.uk
Centre for Advanced Powertrain and Fuels Research
College of Engineering, Design and Physical Sciences
Brunel University London
Kingston Lane
Uxbridge
Middlesex UB8 3PH
United Kingdom

Acknowledgments

Dr Wei Guan would like to acknowledge the Guangxi Yuchai Machinery Company for supporting his PhD study supervised by Prof. Hua Zhao at Brunel University London.

Declaration of conflicting interests

The author(s) declared no potential conflicts of interest with respect to the research, authorship, and/or publication of this article.

Definitions/Abbreviations

ATDC	After Firing Top Dead Center.
CA90	Crank Angle of 90% Cumulative Heat Release.
CA50	Crank Angle of 50% Cumulative Heat Release.
CA10	Crank Angle of 10% Cumulative Heat Release.
CA10-CA50	10–50% Cumulative Heat Release.
CA50-CA90	50–90% Cumulative Heat Release.
CA10-CA90	10–90% Cumulative Heat Release.
CAD	Crank Angle Degree.
CLD	Chemiluminescence Detector.
CO	Carbon Monoxide.
CO_2	Carbon Dioxide.

COV_IMEP	Coefficient of Variation of IMEP.
DAQ	Data Acquisition.
DF	Dual-Fuel.
DOC	Diesel Oxidation Catalyst.
DMDF	Diesel-Methanol Dual-Fuel.
ECR	Effective Compression Ratio.
ECU	Electronic Control Unit.
EGR	Exhaust Gas Recirculation.
EIVC	Early Intake Valve Closing.
FID	Flame Ionization Detector.
FSN	Filter Smoke Number.
GHG	Greenhouse Gas.
HCCI	Homogenous Charge Compression Ignition.
HRR	Heat Release Rate.
HC	Hydrocarbons.
HD	Heavy Duty.
IMEP	Indicated Mean Effective Pressure.
IVO	Intake Valve Opening.
IVC	Intake Valve Closing.
ISsoot	Net Indicated Specific Emissions of Soot.
$\mathbf{ISNO_x}$	Net Indicated Specific Emissions of NOx.
ISCO	Net Indicated Specific Emissions of CO.
ISHC	Net Indicated Specific Emissions of Unburned HC.
LIVC	Late Intake Valve Closing.
$\mathbf{LHV_{CO}}$	Lower Heating Value of Carbon Monoxide
$\mathbf{LHV_{DF}}$	Actual Lower Heating Value in Dual-Fuel Mode.
$\mathbf{LHV_{Diesel}}$	Lower Heating Value of Diesel.
$\mathbf{LHV_{methanol}}$	Lower Heating Value of Methanol.
LTC	Low Temperature Combustion.
MFB	Mass Fraction Burned.
MF	Methanol Energy Fraction.
MK	Modulated Kinetics.
$\dot{m}_{methanol}$	Methanol Flow Rate.

$\dot{m}_{diesel}$	Diesel Flow Rate.
NDIR	Non-Dispersive Infrared Absorption.
NIE	Net Indicated Efficiency.
NO_x	Nitrogen Oxides.
P_{int}	Net Indicated Power.
PFI	Port Fuel Injector.
PM	Particulate Matter
P_{max}	Maximum In-cylinder gas pressure.
PCCI	Premixed Charge Compression Ignition.
PPCI	Partially Premixed Charge Compression Ignition.
PRR	Pressure Rise Rate.
RCCI	Reactivity Controlled Compression Ignition.
SCR	Selective Catalytic Reduction.
SOI	Start of Injection.
SOI_main	Main Injection Timing.
SOC	Start of Combustion.
TDC	Firing Top Dead Centre.
T_{int}	Intake air temperature.
UNIBUS	Uniform Bulky Combustion System.
V_{ivc_eff}	Effective Cylinder Volume.
V_{tdc}	Cylinder Volume at TDC.
VVA	Variable Valve Actuation.
θ	Crank Angle Degree.
γ	Ratio of Specific Heats.

References

1. Pachauri, R.K., "Climate Change 2014 Synthesis Report," *Russ. Fed. Hoesung Lee (Republic Korea) Scott B. Power N.H. Ravindranath* 167, 2014, doi:10.1017/CBO9781107415324.

2. SMMT, "New Car CO 2 Report 2018," 2018.

3. Gravel, R., "Freight Mobility and SuperTruck," 2016.

4. Heywood J.B, “Internal Combustion Engine Fundamentals,” ISBN 007028637X, 1988.

5. Barbosa, F.C., “Heavy Duty Emission Standards Assessment - An Engine and Aftertreatment Technological Approach,” *SAE Tech. Pap.*, 2016, doi:10.4271/2016-36-0167.

6. Bendu, H. and Murugan, S., “Homogeneous charge compression ignition (HCCI) combustion: Mixture preparation and control strategies in diesel engines,” *Renew. Sustain. Energy Rev.* 38:732–746, 2014, doi:10.1016/j.rser.2014.07.019.

7. Shi, L., Zhang, L., Deng, K., Lv, X., and Fang, J., “Experimental Research on Mixture Distribution of Diesel Premixed Low-Temperature Combustion,” 8, 2015, doi:10.4271/2015-01-1839.

8. Musculus, M.P.B., Miles, P.C., and Pickett, L.M., “Conceptual models for partially premixed low-temperature diesel combustion,” Elsevier Ltd, ISBN 0360-1285, 2013, doi:10.1016/j.pecs.2012.09.001.

9. Kimura, S., Aoki, O., Ogawa, H., Muranaka, S., and Enomoto, Y., “New Combustion Concept for Ultra-Clean and High-Efficiency Small DI Diesel Engines,” (724), 1999, doi:10.4271/1999-01-3681.

10. Hasegawa, R. and Yanagihara, H., “HCCI Combustion in DI Diesel Engine,” *SAE Tech. Pap. Ser.* 1, 2010, doi:10.4271/2003-01-0745.

11. Reitz, R.D., “Directions in internal combustion engine research,” *Combust. Flame* 160(1):1–8, 2013, doi:10.1016/j.combustflame.2012.11.002.

12. Benajes, J., Molina, S., García, A., Belarte, E., and Vanvolsem, M., “An investigation on RCCI combustion in a heavy duty diesel engine using in-cylinder blending of diesel

and gasoline fuels," *Appl. Therm. Eng.* 63(1):66–76, 2014, doi:10.1016/j.applthermaleng.2013.10.052.

13. Paykani, A., Kakaee, A.H., Rahnama, P., and Reitz, R.D., "Progress and recent trends in reactivity-controlled compression ignition engines," *Int. J. Engine Res.* 17(5):481–524, 2016, doi:10.1177/1468087415593013.

14. Wang, B., Yao, A., Yao, C., Chen, C., Lu, H., and Feng, J., "Experimental investigation on methanol auto-ignition in a compression ignition engine under DMDF mode," *Fuel* 237(92):133–141, 2019, doi:10.1016/j.fuel.2018.09.154.

15. Verhelst, S., Turner, J.W., Sileghem, L., and Vancoillie, J., "Methanol as a fuel for internal combustion engines," *Prog. Energy Combust. Sci.* 70:43–88, 2019, doi:10.1016/j.pecs.2018.10.001.

16. Varde, K.S., "Ignition Delay and Emissions Characteristics of a Methanol-Diesel Fueled Engine at Low Charge Temperatures," *SAE Tech. Pap. Ser.* 1, 2010, doi:10.4271/920037.

17. Hanson, R.M., Kokjohn, S.L., Splitter, D.A., and Reitz, R.D., "An Experimental Investigation of Fuel Reactivity Controlled PCCI Combustion in a Heavy-Duty Engine," *SAE Int. J. Engines* 3(1):2010-01–0864, 2010, doi:10.4271/2010-01-0864.

18. Kokjohn, S.L. and Reitz, R.D., "Characterization of Dual-Fuel PCCI Combustion in a Light-Duty Engine Department of Mechanical Engineering University of Wisconsin - Madison," (July), 2009.

19. Kokjohn, S.L., Hanson, R.M., Splitter, D.A., and Reitz, R.D., "Fuel reactivity controlled compression ignition (RCCI): A pathway to controlled high-efficiency clean

combustion," *Int. J. Engine Res.* 12(3):209–226, 2011, doi:10.1177/1468087411401548.

20. Pedrozo, V.B., May, I., Guan, W., and Zhao, H., "High efficiency ethanol-diesel dual-fuel combustion: A comparison against conventional diesel combustion from low to full engine load," *Fuel* 230(February):440–451, 2018, doi:10.1016/j.fuel.2018.05.034.

21. Reitz, R.D. and Duraisamy, G., "Review of high efficiency and clean reactivity controlled compression ignition (RCCI) combustion in internal combustion engines," *Prog. Energy Combust. Sci.* 46:12–71, 2015, doi:10.1016/j.pecs.2014.05.003.

22. Molina, S., García, A., Pastor, J.M., Belarte, E., and Balloul, I., "Operating range extension of RCCI combustion concept from low to full load in a heavy-duty engine," *Appl. Energy* 143:211–227, 2015, doi:10.1016/j.apenergy.2015.01.035.

23. Asad, U. and Zheng, M., "Exhaust gas recirculation for advanced diesel combustion cycles," *Appl. Energy* 123:242–252, 2014, doi:10.1016/j.apenergy.2014.02.073.

24. Ladommatos, N., Abdelhalim, S.M., Zhao, H., and Hu, Z., "The Dilution , Chemical , and Thermal Effects of Exhaust Gas Recirculation on Diesel Engine Emissions - Part 4 : Effects of Carbon Dioxide and Water Vapour," (412), 1997.

25. Hanson, R., Ickes, A., and Wallner, T., "Comparison of RCCI Operation with and without EGR over the Full Operating Map of a Heavy-Duty Diesel Engine," *SAE Tech. Pap.* (x), 2016, doi:10.4271/2016-01-0794.

26. Wu, Y. and Reitz, R.D., "Effects of Exhaust Gas Recirculation and Boost Pressure on Reactivity Controlled Compression Ignition Engine at High Load Operating Conditions," *J. Energy Resour. Technol.* 137(3):032210, 2015, doi:10.1115/1.4029866.

27. Kavuri, C. and Kokjohn, S., "Investigating Air Handling Requirements of High Load Low Speed Reactivity Controlled Compression Ignition (RCCI) Combustion," 2016, doi:10.4271/2016-01-0782.Copyright.

28. Duraisamy, G., Rangasamy, M., and Nagarajan, G., "Effect of EGR and Premixed Mass Percentage on Cycle to Cycle Variation of Methanol/Diesel Dual Fuel RCCI Combustion," *SAE Tech. Pap. Ser.* 1(x), 2019, doi:10.4271/2019-26-0090.

29. Benajes, J., Pastor, J. V., García, A., and Boronat, V., "A RCCI operational limits assessment in a medium duty compression ignition engine using an adapted compression ratio," *Energy Convers. Manag.* 126:497–508, 2016, doi:10.1016/j.enconman.2016.08.023.

30. Pedrozo, V.B. and Zhao, H., "Improvement in high load ethanol-diesel dual-fuel combustion by Miller cycle and charge air cooling," *Appl. Energy* 210(March 2017):138–151, 2018, doi:10.1016/j.apenergy.2017.10.092.

31. Kumar, C., Rana, K.B., and Tripathi, B., "Effect of diesel-methanol-nitromethane blends combustion on VCR stationary CI engine performance and exhaust emissions," *Environ. Sci. Pollut. Res.* 6517–6531, 2019, doi:10.1007/s11356-018-04058-1.

32. Guan, W., Pedrozo, V., Zhao, H., Ban, Z., and Lin, T., "Exploring the NOx Reduction Potential of Miller Cycle and EGR on a HD Diesel Engine Operating at Full Load," *SAE Tech. Pap.* 2018-April:1–12, 2018, doi:10.4271/2018-01-0243.

33. Martins, M.E.S. and Lanzanova, T.D.M., "Full-load Miller cycle with ethanol and EGR: Potential benefits and challenges," *Appl. Therm. Eng.* 90:274–285, 2015, doi:10.1016/j.applthermaleng.2015.06.086.

34. Zhao, J., “Research and application of over-expansion cycle (Atkinson and Miller) engines ??? A review,” *Appl. Energy* 185:300–319, 2017, doi:10.1016/j.apenergy.2016.10.063.

35. Benajes, J., Serrano, J.R., Molina, S., and Novella, R., “Potential of Atkinson cycle combined with EGR for pollutant control in a HD diesel engine,” *Energy Convers. Manag.* 50(1):174–183, 2009, doi:10.1016/j.enconman.2008.08.034.

36. Guan, W., Pedrozo, B., Zhao, H., Ban, Z., and Lin, T., “Variable valve actuation – based combustion control strategies for efficiency improvement and emissions control in a heavy-duty diesel engine,” *Int. J. Engine Res.*, 2019, doi:10.1177/1468087419846031.

37. Ickes, A., Hanson, R., and Wallner, T., “Impact of Effective Compression Ratio on Gasoline-Diesel Dual-Fuel Combustion in a Heavy-Duty Engine Using Variable Valve Actuation,” *SAE Tech. Pap. Ser.* 1, 2015, doi:10.4271/2015-01-1796.

38. Pan, W., Yao, C., Han, G., Wei, H., and Wang, Q., “The impact of intake air temperature on performance and exhaust emissions of a diesel methanol dual fuel engine,” *Fuel* 162:101–110, 2015, doi:10.1016/j.fuel.2015.08.073.

39. Stricker, K., Kocher, L., Koeberlein, E., Alstine, D. Van, and Shaver, G.M., “Estimation of effective compression ratio for engines utilizing flexible intake valve actuation,” *Proc. Inst. Mech. Eng. Part D J. Automob. Eng.* 226(8):1001–1015, 2012, doi:10.1177/0954407012438024.

40. Pedrozo, V., “An experimental study of ethanol-diesel dual-fuel combustion for high efficiency and clean heavy-duty engines,” PhD Thesis, Brunel University London, 2017.

41. Cheng, K.K. and W.K., “Speciated Engine-Out Organic Gas Emissions from a PFI-SI Engine Operating on Ethanol/Gasoline Mixtures,” *SAE Int. J. Fuels Lubr.* 2,(No. 2 (2010),):91–101, 2010, doi:10.4271/2009-01-2673.

42. AVL., “AVL 415SE Smoke Meter,” *Prod. Guid. Graz, Austria;* 1–4, 2013.

43. Regulation No 49 – uniform provisions concerning the measures to be taken against the emission of gaseous and particulate pollutants from compression-ignition engines and positive ignition engines for use in vehicles. Off J Eur Union, 2013.

44. Zhao, H., “HCCI and CAI engines for the automotive industry,” ISBN 9781855737426, 2007.

45. Prashant, G.K., Lata, D.B., and Joshi, P.C., “Investigations on the effect of methanol blend on the combustion parameters of dual fuel diesel engine,” *Appl. Therm. Eng.* 103:187–194, 2016, doi:10.1016/j.applthermaleng.2016.04.061.

46. Li, Y., Jia, M., Liu, Y., and Xie, M., “Numerical study on the combustion and emission characteristics of a methanol/diesel reactivity controlled compression ignition (RCCI) engine,” *Appl. Energy* 106(x):184–197, 2013, doi:10.1016/j.apenergy.2013.01.058.

47. Authorities, A., “Acts Adopted By Bodies Created By International Agreements,” *Off. J. Eur. Union* 7–9, 2013.

48. Pedrozo, V.B., May, I., Lanzanova, T.D.M., and Zhao, H., “Potential of internal EGR and throttled operation for low load extension of ethanol–diesel dual-fuel reactivity controlled compression ignition combustion on a heavy-duty engine,” *Fuel* 179:391–405, 2016, doi:10.1016/j.fuel.2016.03.090.

Appendix A. Test cell measurement devices

Variable	Device	Manufacturer	Measurement range	Linearity/Accuracy
Speed	AG 150 Dynamometer	Froude Hofmann	0-8000 rpm	± 1 rpm
Torque	AG 150 Dynamometer	Froude Hofmann	0-500 Nm	± 0.25% of FS
Diesel flow rate (supply)	Proline promass 83A DN01	Endress+Hauser	0-20 kg/h	± 0.10% of reading
Diesel flow rate (return)	Proline promass 83A DN02	Endress+Hauser	0-100 kg/h	± 0.10% of reading
Intake air mass flow rate	Proline t-mass 65F	Endress+Hauser	0-910 kg/h	± 1.5% of reading
In-cylinder pressure	Piezoelectric pressure sensor Type 6125C	Kistler	0-300 bar	≤ ± 0.4% of FS
Intake and exhaust pressures	Piezoresistive pressure sensor Type 4049A	Kistler	0-10 bar	≤ ± 0.5% of FS
Oil pressure	Pressure transducer UNIK 5000	GE	0-10 bar	< ± 0.2% FS
Temperature	Thermocouple K Type	RS	233-1473K	≤ ± 2.5 K
Intake valve lift	S-DVRT-24 Displacement Sensor	LORD MicroStrain	0-24 mm	± 1.0% of reading using straight line
Smoke number	415SE	AVL	0-10 FSN	-
Fuel injector current signal	Current Probe PR30	LEM	0-20A	± 2 mA